IEEE Access
Multidisciplinary | Rapid Review | Open Access Journal

Received 9 November 2022, accepted 17 November 2022, date of publication 24 November 2022,
date of current version 1 December 2022.

Digital Object Identifier 10.1109/ACCESS.2022.3224722

RESEARCH ARTICLE

Robust Adaptive Path Tracking Control Scheme for Safe Autonomous Driving via Predicted Interval Algorithm

CONG PHAT VO[1], JUNGEUN LEE[1], AND JEONG HWAN JEON[1,2]
[1]Department of Electrical Engineering, Ulsan National Institute of Science and Technology (UNIST), Ulsan 44919, Republic of Korea
[2]Graduate School of Artificial Intelligence, Ulsan National Institute of Science and Technology (UNIST), Ulsan 44919, Republic of Korea

Corresponding author: Jeong Hwan Jeon (jhjeon@unist.ac.kr)

This work was supported by the 2019 Research Fund (1.190148.01) of UNIST (Ulsan National Institute of Science Technology).

ABSTRACT This paper introduces a robust adaptive path-tracking control scheme via a predicted interval approach for safe autonomous driving tasks under uncertainties. Specifically, a recursive least squares-based set-membership mechanism is firstly designed to estimate a bounding set of acceptable values to depict the uncertain parameters. Based on the estimated system parameters, an interval predictor is deployed to improve the prediction accuracy in the primary control action design. Successively, the unconstrained output feedback-based robust controller is proposed to yield the closed-loop system stabilization by utilizing predicted interval output only. Meanwhile, a model predictive control technique is conceived from solving an optimization problem that is given in the interval predictor to ensure robust constraint satisfaction. The recursive feasibility of the controlled system is theoretically analyzed by applying the nonconservative Lyapunov function with a novel structure and the closed-loop system possesses the input-to-state stability criteria. Finally, simulation results are provided to verify the efficacy of the presented strategy under various intricate scenarios. The results show that the suggested controller always maintains its cross-tracking error and longitudinal velocity error at the lowest level even in the most challenging weather scenario.

INDEX TERMS Path tracking control, autonomous vehicle, interval prediction, model predictive control.

I. INTRODUCTION

With the speed of technological advances, autonomous vehicles (AVs) have been intensively invested in both modern military and civilian areas [1]. Creating an autonomous vehicle equipped with a range of advanced functionalities presents significant challenges. One of the fundamental challenges is the trajectory tracking control task for AVs. Many studies have been conducted on this issue [2], [3], [4]. However, related studies often ignore the physical constraints (e.g., workspace restrictions and speed) to mainly focus on developing the feedback control principles that modulate the tracking error. The saturation function [5] and the barrier function [6] are two broad solutions to the aforementioned problem, although using them could compromise the control performance.

Currently, Reinforcement Learning (RL) [7] is one of the active research areas in the domain of applied Machine Learning [8]. Nevertheless, it has hardly been applied to practical applications, since the essence of the RL is based on evaluating targets empirically obtained from trial-and-error and random exploration, i.e., iterative refinements and learning from failures. In addition, it required sufficiently big data from an environment interaction that cannot always be simulated. Thus, they have rarely been applied to practical vehicle control as of the present since mistakes must be thoroughly avoided for safety.

A hint for these drawbacks is that the control approaches should partially know the dynamic model. Even though they have to face model uncertainties such as unknown

The associate editor coordinating the review of this manuscript and approving it for publication was Yiqi Liu.

parameters and exogenous disturbances, the simple efficiencies of model-based counterparts have often benefited better than model-free counterparts. To leverage the advantages from the model knowledge, a model predictive control (MPC) technique has been efficiently employed for control purposes of real works [9], [10]. The MPC technique not only addresses multi-input multi-output systems but also deals with online constrained optimization problems. It delivers the capability of predicting vehicle behaviors, improving safety as well as controlling performance by looking at several steps in the future. To mention a few, a nonlinear MPC (NMPC) scheme is presented in [11] for nonholonomic systems to ensure system stability. In [12], Li et al. developed the NMPC scheme with a neurodynamic optimization to enhance the computational efficiency for tracking and formation. However, the uncertainty term is ignored in the abovementioned approaches, which are unavoidable in actual AV applications.

Regarding the above restriction, a robust MPC (RMPC) approach is an improved form of the standard MPC. It is intrinsically robust to uncertainties given the tight system constraints. In [13], an RMPC scheme is proposed to handle constraints explicitly of bounded external disturbances. Similarly, a tube-based RMPC scheme [14] is another variant, which also tackles external disturbances by the robustness constraint control scheme. In addition, another extension version [15] is designed for constrained linear time-invariant systems that ensure robust exponential stability. It is noteworthy that the uncertainty bound commonly assumes a prior known in the above-mentioned studies. Moreover, they skipped the model mismatch, i.e., the perfectly modeled system is only concerned with external disturbances. This points out that those methods are relatively conservative. Thus, the parametric uncertainty is required to be systematically and exactly respected as to the additive disturbance or to consider the worst-case realization [16]. Nonetheless, another challenge comes from precisely approximating the effects of the parametric uncertainty when the system states distribute over time.

Alternatively, an adaptive MPC (AMPC) is devised as a promising solution, it focuses on the controlled system properties [17], [18]. In [18], the AMPC is developed based on fulfilling the Persistence of Excitation (PE) condition, intending to guarantee the controlled system properties of robust stability, recursive feasibility and estimation convergence. In view of this approach, model-updating strategies are required by estimation/adaptation algorithms to determine the model uncertainty [19] and the constraints during transients [20]. This poses the challenge that a highly accurate estimate of the system state is required, which is often affected by restrictive assumptions. Notwithstanding that, the model information can be obtained by many approaches, which have been introduced in [21], [22], [23], and [24]. A nonlinear disturbance observer (NDO) is a well-known estimation method to utilize for developing controllers against system uncertainties and disturbances. Scholars in [21], [22], and [23] have proposed several NDO versions with extremely robust performance. However, this work focuses on the estimations of unknown parameters and uncertainty sets to regard the conservatism of the MPC algorithms [24]. Thus, the set-membership estimation mechanism based on the recursive least-squares (RLS) technique [25] is deployed to estimate along the way with the bounding sets, which are described by ellipsoids or polytopes. Besides, the weighting factors are relatively easy to be selected at a known interval from zero to infinity. Additionally, instead of deploying a regular solution, the interval predictor is designed to tackle the uncertain system [26], [27], [28], [29], [30]. In detail, the interval prediction technique is the evaluation of the set of acceptable values for the state at each instant. It is practicable based on input-output information. Nonetheless, the addition of time intervals from uncertain elements may affect the system, causing instability. Therefore, the predicted interval mechanism design should take into account the stability and inclusion property.

In this work, we develop a robust adaptive path-tracking control scheme for safe autonomous driving tasks via a predicted interval (PI) algorithm. To start with, the unknown parameters are first estimated along the way by the RLS-based set-membership estimation mechanism. This set estimator yields not only a nonincreasing estimation error but also a sequence of bounding sets where the uncertain parameters can be freely distributed. For the simplicity of implementation and computational efficiency, instead of relying on zonotopes [31], [32], the proposed prediction approach is deployed based on intervals for the system state prediction. Successively, this interval predictor is further exploited for the promising combination of the AMPC-based safety controller and the robust output feedback control (ROFC) strategy. The proposed control scheme is operated in a way that leverages the AMPC technique to reach the vicinity of the origin. Meanwhile, the unconstrained ROFC is immediately executed to maintain the system stabilization that only utilizes the predicted interval variables. The stability of the closed-loop control is theoretically analyzed based on a novel nonconservative Lyapunov function assisted by the conditions of linear matrix inequalities (LMIs). Finally, the effectiveness and feasibility of the proposed algorithm are investigated in high-fidelity simulations with a number of weather scenarios. The key contributions of this work are summarized as follows:

- The RLS-based set-membership estimation mechanism determines the unknown parameters with the nonincreasing estimation error. It delivers the sequence of bounding sets, where the uncertain parameters can be freely expanded.
- A robust adaptive path tracking control scheme is proposed based on the interval predictors for exponentially stabilizable nonlinear systems. The suggested control action design is harmoniously combined between the stabilizing AMPC technique and the unconstrained ROFC framework. It allows us to guarantee the constraint satisfaction and robust system stabilization.

- The stability and recursive feasibility of the controlled system are theoretically analyzed by a novel nonconservative Lyapunov function with the assistance of the LMIs conditions.

The remainder of the paper is organized as follows. Section III describes the dynamic system and objectives. Section IV outlines the design procedure of the proposed approach including the estimator, predictor and controler. Section V describes the simulation scenarios and discusses the results. Finally, the conclusions are summarized in Section VI.

II. NOTATIONS

The symbols $\mathbb{N}$ and $\mathbb{R}$ are sets of natural numbers and real numbers, respectively. Denote $\overline{n} = 1, 2, \ldots, n$, $\forall n \in \mathbb{N}$. The symbol I_n denotes the $n \times n$ identity matrix. For a matrix $A \in \mathbb{R}^{n\times n}$, denote $A^+ = \max\{0, A\}$, $A^- = A^+ - A$ and the absolute values of the matrix as $|A| = A^+ + A^-$. The inputs $u : \mathbb{R}_{\geq 0} \to \mathbb{R}^n$ with $||u||_{\geq 0} < \infty$ is denoted as Γ^n. Given a matrix $P \in \mathbb{R}^{n\times n}$, $P \preceq 0$ implies that a symmetric matrix is negative semi-definite.

III. PROBLEM STATEMENT

In this section, we first formulate the dynamic model of Educational Robot Platform (Wego-ERP42) developed by the WeGo Robotics company [33] for autonomous driving, which is illustrated in Fig. 1, then control objectives of this study are given.

A. DYNAMIC MODEL

The vehicle dynamic model is described by the classical single-track model represented in (1) with a mass m and a yaw moment of inertia I_z. According to Newton's Second Law, the degrees of freedom of the longitudinal and lateral velocities, the yaw angle and the orientation error can be obtained from [34] and [35]. As the results, the vehicle dynamics model is derived as follows:

$$\begin{cases} \dot{v}_x = a - \dfrac{C_f\delta\sin\delta}{m} + \dfrac{C_f(l_f\omega + v_y)\sin\delta}{mv_x} + \omega v_y \\ \dot{v}_y = \dfrac{C_f\delta\cos\delta}{m} - \dfrac{C_f(l_f\omega + v_y)\cos\delta}{mv_x} \\ \qquad + \dfrac{C_r(l_r\omega - v_y)}{mv_x} - \omega v_x \\ \dot{\omega} = \dfrac{l_f C_f\delta\cos\delta}{I_z} - \dfrac{l_f C_f(l_f\omega + v_y)\cos\delta}{I_z v_x} \\ \qquad - \dfrac{l_r C_r(l_r\omega - v_y)}{I_z v_x} \\ \dot{\theta}_e = \omega - \dfrac{v_x\cos\theta_e - v_y\sin\theta_e}{1 - y_e\kappa}\kappa \end{cases} \tag{1}$$

where v_x, v_y, and ω are the dynamic states corresponding to lateral velocity, longitudinal velocity, and yaw angle with the respect to the coordinates of the vehicle (O_x, O_y); θ_e is the orientation error with road curvature κ; y_e is the lateral deviation in the curvilinear frame, i.e., distance from the vehicle center to the closest point p on the desired path; the front steering angle δ and the longitudinal acceleration a are considered as the control actions; C_f/C_r and l_f/l_r are the stiffness coefficients of the tires and the distances from the center of gravity to the front/rear wheel axes, respectively. In cases the longitudinal velocity v_x becomes almost zero, introducing and adding a small constant value ε may alleviate the singularity phenomenon.

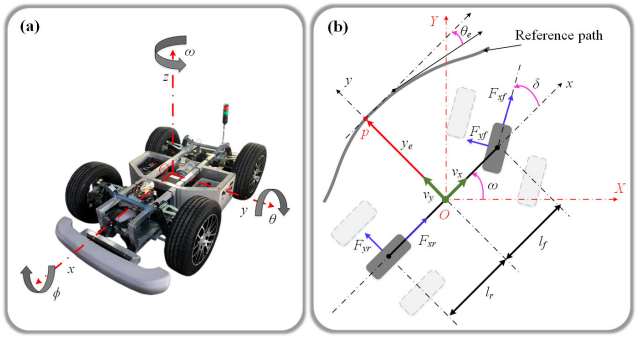

FIGURE 1. The architecture of the testing vehicle; (a) the WeGo-ERP42 was created by the WeGo Robotics company, (b) The dynamic model and its variables with respect to the reference path.

Based on (1), the complete state-space model is given by the formula in time-domain representation as follows:

$$\begin{cases} \dot{x}(t) = A(\xi(t))x(t) + Bu(t) + d(t) \\ y(t) = Cx(t) + \gamma(t) \end{cases} \tag{2}$$

where $x(t) = [v_x, v_y, \omega, \theta_e]^\top \in \mathbb{R}^p$ denotes the vehicle state with an initial state $x(0) = x_0$ and its derivative $\dot{x}(t)$; $u(t) = [\delta, a]^\top \in \mathbb{R}^q$ denotes the control input; $d(t) \in \mathbb{R}^r$ is the external disturbances; $y(t)$ denotes the measurement output; $\gamma(t) \in \mathbb{R}^{2p}$ is the measurement noise; the uncertain variables $\xi(t) = [v_x, v_y, \theta_e, \kappa] \in \mathbb{R}^N$ belongs to a confidence region set $\mathcal{D} \subset \mathbb{R}^d$; time index is $t \in \mathbb{N}$, $\forall t \geq 0$; the system matrices $A \in \mathbb{R}^{p\times p}$, $B \in \mathbb{R}^{p\times q}$ and $C \in \mathbb{R}^{n\times p}$ based on the nonlinear embedding method [36] are derived in Appendix A.

B. CONTROL OBJECTIVE

The objective of this work is to develop a robust adaptive path tracking controller for the system (2) based on the PI technique supported by the online uncertain parameter estimation, where its stabilization and robust constraint satisfactions have to be guaranteed. With the intention of achieving the stabilization of the control system against uncertainties and disturbances in the vicinity of the origin, for all $t \geq 0$, the system (2) is subject to the constraint sets of the state $x(t) \in \mathcal{S} \subset \mathbb{R}^p$ and control $u(t) \in \mathcal{A} \subset \mathbb{R}^q$. In order to obtain an estimated confidence region set $\hat{\mathcal{D}}(t) \subseteq \mathcal{D}$ containing the uncertain parameters ξ, the form of $A(\xi)$ is defined as the following.

Assumption 1: The matrices $A, \rho_1, \ldots, \rho_N \in \mathbb{R}^{p\times p}$ are known existence such that the relations are satisfied $\forall\xi \in \mathcal{D}$

as follows:

$$A(\xi) = A + \sum_{i=1}^{N} \rho_i \xi_i. \tag{3}$$

Assumption 2: In the system (2)*, there exist admissible perturbation bounds* $\underline{d}, \overline{d} \in \Gamma^r$, $\underline{\gamma}, \overline{\gamma} \in \Gamma^{2p}$ *such that* $d \in [\underline{d}(t), \overline{d}(t)], \gamma \in [\underline{\gamma}(t), \overline{\gamma}(t)], \forall t \geq 0$*, both containing the origin in their interior. In addition,* $\underline{x}_0, \overline{x}_0 \in \Gamma^p$ *such that the initial conditions* $x_0 \in [\underline{x}_0, \overline{x}_0] \subset \mathcal{S}$*. The initial uncertainty set is defined by* $\mathcal{D}_0 = \left\{\xi \in \mathbb{R}^N, |\xi - \xi_0| \leq \overline{\xi}\right\}$*, where an initial* ξ_0 *and* $\overline{\xi}$ *are positive values.*

Assumption 1 is given in order to provide the desired solution by the PI approach, which requires a careful selection of hypotheses to ensure robust stability. Different from other methods, the cooperativity and stability of the estimation error dynamics are guaranteed by a suitable choice of weighting factors. In Assumption 2, it is supposed that the perturbations belong to the know bounded interval, which is the standard hypothesis for interval estimation [30]. Further, this assumption indicates the bounded uncertainties. Due to the limit of physical systems, it is normally utilized in the literature on the path tracking problem.

IV. THE PROPOSED CONTROL STRATEGY

In this part, a robust adaptive MPC scheme with an interval predictor is developed for safe autonomous driving. The structure shown in Fig. 2 describes the main modules of the designed control algorithm. As first, an online strategy is first deployed to determine the unknown parameters and the uncertainty set simultaneously. Next, the interval prediction block is developed with the inclusion properties to precompute the information on the observed current states. Later, two primary module blocks are the ROFC block and the AMPC-optimizer block relying on the interval predictor results. Moreover, the final optimal control signal is decided based on the condition of the extended state reaching the vicinity set of origin. The outstanding features of the proposed approach consist of the capability of guaranteeing robust constraint satisfaction from the designed AMPC approach. Meantime, ROFC-based closed-loop control uses the interval predictor variables only, which delivers asymptotic performances with unconstrained stabilizing. The detail of the designed control approach is presented as the following.

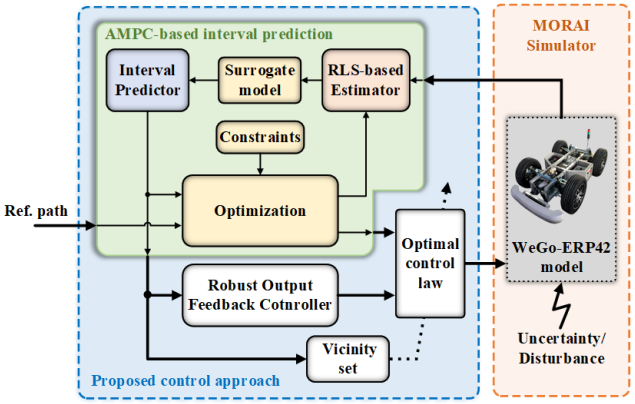

FIGURE 2. Block diagram of the proposed control scheme.

A. PARAMETERS ESTIMATION

In order to derive the uncertainty set for the unknown parameters, we assume that the nominal term $\Lambda(x(t), u(t), \xi)$ without the uncertainty terms is linearly dependent on ξ. To leverage the statistical tools developed for nonasymptotic linear regression, (2) is given by $Y(t) = \Lambda(t)\xi^* + \vartheta(t)$, in which $\Lambda(t) = [\rho_1 x_n(t), \ldots, \rho_N x_n(t)] \in \mathbb{R}^{p\times N}$, $\forall n$ are known signals. A hypothesis on the level of its excitation is introduced in [37] and [38]; ξ^* denotes the true parameter of ξ at time instant t with $\xi^* \in \mathcal{D}(0)$ and $\vartheta(t) = d(t) + \gamma(t)$ is the lumped uncertainty in a regression model, which is from Γ^p under assumptions 1 and 2. It is also implied that $||\vartheta|| \leq \overline{\vartheta}$, with $\overline{\vartheta} = \max\left\{||\underline{d}||, ||\overline{d}||\right\} + \max\left\{||\underline{\gamma}||, ||\overline{\gamma}||\right\}$.

In order to determine $\hat{\mathcal{D}}(t)$, the set-membership technique based on [25] is employed to calculate the estimation vector $\hat{\xi}(t)$ of uncertain parameters $\xi, \forall t \geq 0$, it can be expressed as:

$$\dot{\hat{\xi}}(t) = \hat{\xi}(t) + \dot{\kappa}_e(t)\dot{\breve{\sigma}}(t)\Lambda(t)\dot{\tilde{\vartheta}}(t) \tag{4}$$

where $\hat{\xi}(t) \in \mathbb{R}^N$, $\breve{\sigma}(0) = 1$ and the following equalities:

$$\dot{\tilde{\vartheta}}(t) = Y(t) - \Lambda(t)\hat{\xi}(t) \tag{5a}$$

$$\dot{\breve{\sigma}}(t) = \frac{\breve{\sigma}}{1 + \dot{\kappa}_e(t)\breve{\sigma}\Lambda(t)^2} \tag{5b}$$

$$\dot{\kappa}_e(t) = \begin{cases} 0, & \text{if } \left|\dot{\tilde{\vartheta}}\right| \leq \overline{\vartheta}, \\ \dfrac{\left|\dot{\tilde{\vartheta}}(t)\right| - \xi}{\overline{\vartheta}\Lambda(t)^2\dot{\breve{\sigma}}(t)} & \text{otherwise} \end{cases} \tag{5c}$$

In order to ensure the robust satisfaction of constraint against uncertainties and disturbances, the objective of the following step is to compute an appropriate set of all admissible values $\hat{\mathcal{D}}(t) \subseteq \mathcal{D}$, meaning that $\xi, \hat{\xi}(t) \in \hat{\mathcal{D}}(t), \forall t \geq 0$. Based on (4), the set $\hat{\mathcal{D}}(t)$ can be given as follows:

$$\hat{\mathcal{D}}(t) = \mathcal{D} \bigcap_{\iota\in[\varrho,t]} \left\{\xi^* \in \mathbb{R}^N : |\xi^* - \hat{\xi}(\iota)| \leq \widetilde{\delta}(\iota)\right\} \tag{6}$$

where $\widetilde{\delta}(\iota) = \varpi(\iota)\breve{\sigma}^{\frac{1}{2}}$ in which the expression $\varpi(0) = \overline{\xi}$ and $\varpi(t)$ at time instant t is defined by

$$\dot{\varpi}(t) = \left(\varpi^2(t) + \dot{\kappa}_e\left(\overline{\vartheta}^2 - \frac{\widetilde{\delta}^2}{1 + \dot{\kappa}_e\Lambda^2\breve{\sigma}}\right)\right)^{\frac{1}{2}} \tag{7}$$

It is evident that the property $\hat{\mathcal{D}}(t) \subseteq \mathcal{D}, t \geq 0$ is fulfilled while its size is shrinking. The estimation features can be summarized as the following lemma.

Lemma 1: The true parameter ξ^* *belongs to* $\mathcal{D}(t)$ *and the bounded error* $\widetilde{\xi} = \xi^* - \hat{\xi}(t)$ *of* (4) *is guaranteed to be nonincreasing, for all* $t > 0$ *when Assumptions 1-2 are satisfied.*

Proof: See in Appendix B. ■

B. ROBUST ADAPTIVE PATH TRACKING CONTROL

In this part, we develop a new robustness constraint strategy, which leverages the results obtained from the aforementioned estimations including the current state $x(t)$ belongs to $[y(t) - \underline{\gamma}(t), y(t) + \overline{\gamma}(t)]$ with the initial conditions $[\underline{x}_0, \overline{x}_0]$ and the estimated confidence region $\hat{\mathcal{D}}(t)$, as well as the admissible exogenous bounds $[\underline{d}(t), \overline{d}(t)]$, to generate bounded interval estimates $[\underline{x}(t), \overline{x}(t)] \in \mathbb{R}^p$ such that

$$\underline{x}(t) \leq x(t) \leq \overline{x}(t), \forall t \geq 0. \tag{8}$$

Since the estimated set $\hat{\mathcal{D}}(t)$ is determined by (6) and $\xi \in \hat{\mathcal{D}}(t) \subseteq \mathcal{D}$ while the system matrix A and the set $\mathcal{D}$ are known, then there exist the bounded matrices $\underline{A}, \overline{A}$:

$$\underline{A} \leq A(\xi) \leq \overline{A} \tag{9}$$

According to Assumption 1, the confidence region $\hat{\mathcal{D}}(t)$ can be enclosed on ξ obtained from (6) into a polytope for $A(\xi)$, which can be expressed as follows:

$$A(\xi) = A_0 + \sum_{i=1}^{2^N} \chi_i \Xi_i \tag{10}$$

where $A_0 = A(\hat{\xi}(t))$, $\chi \geq 0$, $\sum_{i=1}^{2^N} \chi_i = 1$, $\Xi_i = A(\hat{\xi} + k_i\widetilde{\delta}) - A_0$ for $k_i \in \{-1, 1\}^N$ with $i \in 2^N$. In addition, to inherit beneficial features of nonnegative systems, all the off-diagonal components of the center matrix A_0 are nonnegative, i.e., it is Metzler.

Assumption 3: There exists a nonsingular matrix $H \in \mathbb{R}^{p\times p}$ with $H^{-1}A_0H$ being Metzler.

In fact, the above assumption is frequently satisfied whenever A_0 is a diagonalizable matrix or a scalar output system can be observed [39]. Additionally, suppose that $H = I_p$ in order to decompose the notation and ensure that the system (2) is already in the correct form:

$$\dot{x}(t) = \left(A_0 + \sum_{i=1}^{2^N} \chi_i \Xi_i\right) x(t) + Bu(t) + d(t) \tag{11}$$

To obtain the new states at time τ, with $\tau \leq t$, while still guaranteeing the bounded feature 9, the interval predictor is designed as follows:

$$\begin{cases} \dot{\underline{x}}(\tau) = A_0\underline{x}(\tau) - \Xi^+\underline{x}^-(\tau) - \Xi^-\overline{x}^+(\tau) \\ \qquad + Bu(\tau) + \underline{d}(\tau) - \overline{d}(\tau), \\ \dot{\overline{x}}(\tau) = A_0\overline{x}(\tau) - \Xi^+\overline{x}^-(\tau) - \Xi^-\underline{x}^+(\tau) \\ \qquad + Bu(\tau) + \overline{d}(\tau) - \underline{d}(\tau) \end{cases} \tag{12}$$

where the polynomials $\Xi^+ = \sum_{i=1}^{2^N} \Xi_i^+$, $\Xi^- = \sum_{i=1}^{2^N} \Xi_i^-$.

In order to integrate the interval predictor (12) into the suggested robust control scheme, we define the extended state vector of the predictors as $X = [\underline{x}^\top, \overline{x}^\top]^\top$, then the equation (11) can be rewritten as follows:

$$\dot{X}(t) = \eta_1 X(t) + \eta_2 X^+(t) - \eta_3 X^-(t) + \beta u(t) + \psi(t) \tag{13}$$

where $\psi(t) = [\underline{d}(t), \overline{d}(t)]^\top \in \mathbb{R}^{2p}$ is a bounded input vector. Its norm is in the ratio to $\underline{d}, \overline{d}$ and $\eta_1 = \begin{bmatrix} A_0 & 0 \\ 0 & A_0 \end{bmatrix}$, $\eta_2 = \begin{bmatrix} 0 & -\Xi^- \\ 0 & \Xi^+ \end{bmatrix}$, $\eta_3 = \begin{bmatrix} -\Xi^+ & 0 \\ \Xi^- & 0 \end{bmatrix}$, $\beta = [B^\top, B^\top]^\top$. Since the existence of $X^+(t)$ and $X^-(t)$ is the globally Lipschitz nonlinearities in (13), thus this equation is considered a nonlinear system.

According to (8), the bounded property of $X(t)$ is equivalent to the property of $x(t)$. With the purpose of the input-to-state stabilizers, the asymptotic amplitude of the extended state $X(t)$ with regard to $\psi(t)$ [40] is obtained from the proposed robust output feedback control $u(t) \in \mathcal{A}$, which is designed as follows:

$$u(t) = \kappa_1 X(t) + \kappa_2 X^+(t) - \kappa_3 X^-(t) + \mho\psi(t) \tag{14}$$

where κ_j for $j = (1, 2, 3)$ and $\mho \in \mathbb{R}^{q\times 2p}$ are the control gains. Minimizing $||\beta\mho + I_{2p}||$, $\mho$ is easily chosen. Substituting the control law (14) into the closed-loop system (13), the form can be obtained as follows:

$$\dot{X}(t) = \upsilon_1 X(t) + \upsilon_2 X^+(t) - \upsilon_3 X^-(t) + \widetilde{\psi}(t) \tag{15}$$

where $\widetilde{\psi}(t) = (\beta\mho + I_{2p})\psi(t)$ and $\upsilon_j = \beta\kappa_j + \eta_j$, and the control gains κ_j can be determined as follows.

Theorem 1: Suppose that there exists diagonal matrices G, G^+, G^-, P, G_c, G_c^+, G_c^-, F, F^+, F^-, F_c, F_c^+, F_c^-, H^+, H^-, $L \in \mathbb{R}^{2p\times 2p}$ and matrices $K_j \in \mathbb{R}^{q\times 2p}$ such that P, H^+, H^-, L are positive definite, while Ω, Ψ (see in Appendix C) are negative semi-definite and the following inequalities hold:

$$P + \min\left\{H^+, H^-\right\} > 0, \tag{16a}$$
$$G + \min\left\{G^+, G^-\right\} + 2\min\left\{F^+, F^-\right\} > 0, \tag{16b}$$
$$G_c + \min\left\{G_c^+, G_c^-\right\} + 2\min\left\{F_c^+, F_c^-\right\} > 0, \tag{16c}$$

then the closed-loop system (15) driven by the proposed control signal $u(t)$ with the control gains $\kappa_1 = K_1P$, $\kappa_1 = K_2H^+$, $\kappa_3 = K_3H^-$ is input-to-state stability (ISS) [41] with regard to $(\underline{d}, \overline{d})$.

Proof: See in Appendix C. ■

Remark 1: The existence of a diagonal solution of symmetric matrix P in $\upsilon_1^\top P + P\upsilon_1 \preceq 0$ in [42] and the stability of a Metzler matrix υ_1 are equivalent, thus the matrix P has to be diagonally unrestricted.

Based on the candidate Lyapunov function $V_2(X)$ in the proof of Theorem 1, all trajectories in (13) are asymptotically shrunk in the vicinity set, which is determined as follows:

$$\mathcal{R} = \left\{X \in \mathbb{R}^{2p} : V_2(X) \leq \frac{1}{\Upsilon}\sup_{t\geq 0}\left|\widetilde{\psi}^\top(t)L\widetilde{\psi}(t)\right|\right\} \tag{17}$$

where $\Upsilon = \min_{i\in 2p}\lambda_i(\frac{\Theta}{P+H^++H^-})$ with a scalar value $\lambda(\bullet)$ is an eigenvalue of $(\bullet)$ and the term Θ is the sum of the diagonal matrices in the inequality (16b).

According to Theorem 1, the suggested control signal (14) enables the predictive scheme (12) and its stability in an

area $\mathcal{R}$ of the origin. Meantime, the size of $\mathcal{R}$ is in the ratio to the uncertainty in the system (2). This can be optimized by the selection of κ_i. We developed a new robust adaptive path tracking control strategy to deal with the error between the anticipated output variables and the reference values as little as possible, allowing for precise trajectory tracking and lateral stability for the vehicles. This was done to assure the robust satisfaction of constraints. Given the bounded constraint sets for the state $x(t) \in \mathcal{S}$ and the control $u(t) \in \mathcal{A}$, the control problem would be resolved based on (8), which also causes the system (12) to approach the vicinity of the origin. Denoting the time step T_m and $t_s = sT_m, \forall s \in \mathbb{N}^+$, and the prediction horizon of the MPC solution is denoted as $T_p > T_m$. It means that an optimal control issue at each nonnegative t_s is solved on the interval $[t_s, t_s+T_p]$ to compute the input $u(t)$, and this optimal control issue is resolved again after T_m units of time, i.e., the obtained optimal control is executed on the interval $[t_s, t_s + T_m)$. The objective function can be constructed as follows:

$$\begin{aligned} &J(X(t_s), u(t_s)) \\ &\quad = X^\top \left(t_s + T_p\right) \omega_1 X(t_s + T_p) \\ &\qquad + \int_{t_s}^{t_s+T_p} X^\top(\tau)\omega_2 X(\tau) + u^\top(\tau)\omega_3 u(\tau) d\tau \end{aligned} \tag{18}$$

where $\omega_i \succeq 0 \in \mathbb{R}^{2p\times 2p}$ are the weight gains as positive definite symmetric matrix structures. In order to react against the influence of great measurement disturbances, the bounded estimation at t_s is given as follows:

$$\begin{aligned} &[\underline{x}(t_s), \overline{x}(t_s)] \\ &\quad = \begin{cases} [y(t_s) - \underline{\gamma}(t_s), y_(t_s) + \overline{\gamma}(t_s)] \\ \quad \cap [\underline{x}_0, \overline{x}_0], & s = 0 \\ [y(t_s) - \underline{\gamma}(t_s), y_(t_s) + \overline{\gamma}(t_s)] \\ \quad \cap [\underline{x}(t_{s-1} + T_m), \overline{x}(t_{s-1} + T_m)], & s \geq 1 \end{cases} \end{aligned} \tag{19}$$

where $(\underline{x}^\top(t_{s-1} + T_m), \overline{x}^\top(t_{s-1} + T_m))^\top = \xi(t_{s-1} + T_m)$ is obtained during the prediction on the previous iteration.

Firstly taking $\hat{\mathcal{D}}(t_s)$ from (6) and calculating the matrices A_0 and Ξ_i calculated in (10) with $i \in \overline{2N}$, then the interval prediction-based robust adaptive path tracking control scheme can be formulated by the finite horizon optimal control issue as follows:

$$\begin{aligned} &\Delta U(t_s) \\ &= \underset{u:[t_s,t_s+T_m]\to\mathbb{R}^q}{\operatorname{argmin}} \quad J(X(t_s), u(t_s)) \\ &\qquad \text{s. t. } X : [t_s, t_s + T_m] \to \mathbb{R}^{2p} \\ &\qquad\quad \text{is a solution of (4) and (19)}, \\ &\qquad\quad X(t_s + T_m) \in \mathcal{R}, \\ &\qquad\quad X(\tau) \in \mathcal{S}^2,\ u(\tau) \in \mathcal{A},\ \forall \tau \in [t_s, t_s + T_m]. \end{aligned} \tag{20}$$

By solving the optimization problem (20), the sequence of optimal input deviations computed at time $t \in [t_s, t_s + T_m)$ and the gains control κ_j are taken from (14). Subsequently, either the proposed robust feedback control or the suggested AMPC-based interval prediction is utilized in the final optimal control design. The preferred command is induced by the dependence relationship between the extended state $X(t)$ and the vicinity set $\mathcal{R}$, which is manifested as

$$u(t) = \begin{cases} u(t) & \text{if } X(t_s) \in \mathcal{R}, \\ \Delta U(t) & \text{Otherwise.} \end{cases} \tag{21}$$

Remark 2: Based on [15] and [43], the proposed control scheme is established on the orchestration idea of switching between the AMPC technique and the ROFC approach which both exploit the predicted intervals. In detail, the AMPC-based open-loop optimal control as a safety controller is to guarantee a robust constraint satisfaction for the state $x(t) \in \mathcal{S}$ by reaching a neighborhood of the origin $\mathcal{R}$. Meanwhile, the ROFC-based closed-loop robust controller with the control signal $u(t) \in \mathcal{A}$ in (14) can be applied where the extended states $X(t)$ are inside the vicinity set $\mathcal{R}$ in (17) to maintain robust closed-loop stability, which provides asymptotic performances.

In addition, the initial prediction condition (19) is chosen in a way to use all available information about the state, which means that the set is an intersection of the measured interval $[y(t_s) - \underline{\gamma}(t_s), y(t_s) + \overline{\gamma}(t_s)]$ and the set $[\underline{x}_0, \overline{x}_0]$ at $t_0 = 0$ (according to Assumption 2). Next, we again take the measured information and project it into the interval $[\underline{x}(t_{s-1} + T_m), \overline{x}(t_{s-1} + T_m)]$ at t_s with $s \geq 1$, which is the predicted set of admissible values of $x(t_s)$ at t_{s-1} with the switched optimal control (21). Since the construction of the inclusion property (8) is always satisfied for the predictor (12), the crossing of $[y(t_s) - \underline{\gamma}(t_s), y(t_s) + \overline{\gamma}(t_s)]$ (measured currently) with $[\underline{x}(t_{s-1} + T_m), \overline{x}(t_{s-1} + T_m)]$, at T_m units of time ago, may reduce the influence of $\gamma(t)$.

Theorem 2: Under Assumptions 1-3 and the conditions of Theorem 2, when having $\underline{x}_0, \overline{x}_0 \in \mathcal{S}$, i.e., the boundedness of the unknown parameter estimation in Lemma 1, the closed-loop system presented in (2) possesses both the ISS criterion with respect to $\underline{x}, \overline{x}$ and the practical ISS criterion for x about $\underline{d}, \overline{d}$ in the vicinity set $\mathcal{R}$. Moreover, not only robust constraint satisfaction but also recursive feasibility of the proposed control scheme are guaranteed with reaching $\mathcal{R}$ in a finite time.

Proof: See in Appendix D. ■

Remark 3: Lemma 1, Theorems 1 and 2 imply that the proposed control scheme can absolutely ensure recursive feasibility and closed-loop stability, depending on a conservative bound on the admissible uncertainties. A potential solution to reduce the conservatism of the proposed method is to update the vicinity set, which guarantees the estimation error to be nonincreasing. It is clear from Theorem 2 that the considered system free of disturbances can be stabilized for arbitrarily parametric uncertainty and additive disturbances.

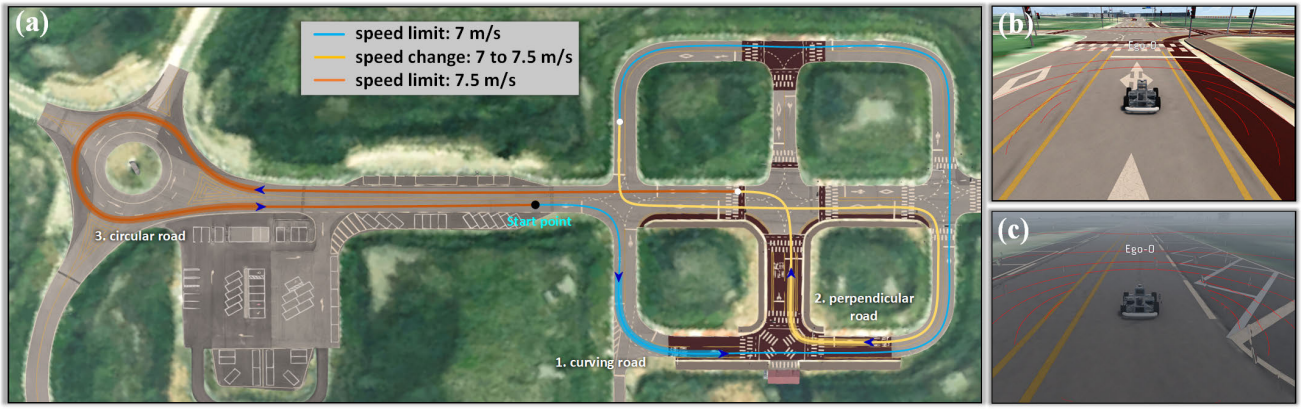

FIGURE 3. Various conditions in the MORAI simulation environment; (a) Top view, the weather scenarios as (b) Sunny, (c) Storm.

V. SIMULATION VALIDATION

A. ENVIRONMENT SETUP

To evaluate the robustness and effectiveness of the suggested control algorithm for safe autonomous driving, our plan is to conduct a series of trials on the WeGo-ERP42 [33], first using a MORAI simulator [44] in various environment settings while still ensuring the safety for extreme conditions. It is a high-fidelity simulation environment based on actual data logs from deployed vehicles that provide both typical and realistic urban layouts under various real scenarios, as shown in Fig. 3 with different weather conditions. Specifically, Fig. 3 (a) shows a top view of route selection for the trials, which is challenging on 1) curving road with large curvature, 2) perpendicular road and 3) circular road in the roundabout. Moreover, the vehicle enters the road with a target speed is 7 m/s on a light blue segment, then increases speed from 7 m/s to 7.5 m/s on a light yellow segment, and reaches the speed of 7.5 m/s on a brown segment. In addition, to generate challenges for path tracking similar to lane-keeping applications, both control strategies are implemented in various weather situations with unknown tire friction. Specifically, the vehicle is operated on a dry road in a Sunny situation, which is considered a relatively "standard" scenario, as seen in Fig. 3 (b). Meanwhile, a Storm situation with heavy rain and winds is considered a "hazardous" scenario. It caused the vehicle frame to be shaken as well as influenced the traction of the wheels on the road due to the slippery road, as seen in Fig. 3 (c).

In order to validate the genuine perspective on the path-tracking efficiency of the proposed methods, the standard MPC in [10] and the RMPC method in [14] are used for comparison purposes. At the point $O(0, 0)$, the vehicle starts to move in the direction with positive coordinates. For the control design, the optimal control issue is solved every sampling period of 20 Hz to find the appropriate control actions and the prediction horizon is chosen as $T_p = 1.25$ s. The front steering angle and longitudinal acceleration of the vehicle are bounded within the limits $\mathcal{A} = \pm\left[\frac{\pi}{4}\ 1.25\right]^\top$ and $\mathcal{S} = \pm\left[8\ 2\ 3\ 10\right]^\top$. Instead of simply tracking the position of the vehicle compared with the reference trajectory, we desire the longitudinal velocity at the profile to change from 7 m/s at 60 s to 7.5 m/s at 100 s. Furthermore, to facilitate the observation of the fluctuations of the results, the standard deviations for each curve in the trial scenarios are calculated by the formulation, $\left(\sqrt{\frac{1}{N_s-1}\sum_{i=1}^{N_t} |\bullet_i - mean(\bullet)|^2}\right)$, where $(\bullet)$ is the data set and N_s is the number of time steps in the population. It is chosen as $N_s = 5$ steps when computing the responses of the cross tracking errors and the longitudinal velocity errors and $N_s = 10$ steps for the optimal control signals.

B. RESULTS

The whole trajectories by the center point O of the WeGo-ERP42 are depicted in Fig. 4 under numerous trial conditions. The simulation time starts to record at the start point corresponding to 0 s in the time axis. It can be observed that the vehicle controlled by the proposed strategy achieved

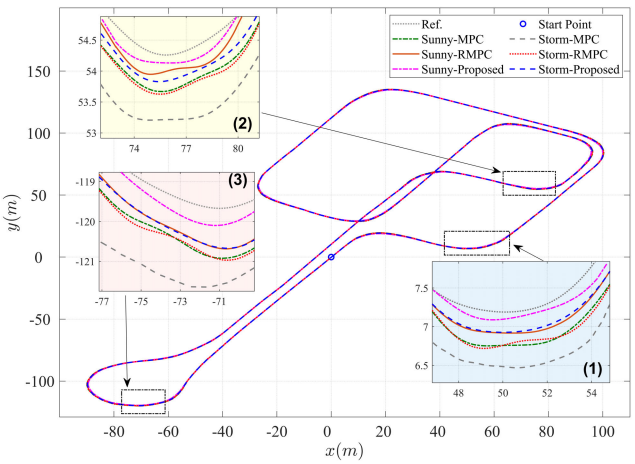

FIGURE 4. Trajectories of the center point $O(t)$ of the testing vehicle.

an extremely high accuracy in which the vehicle path was almost identical to the reference path on straight segment roads (e.x., from 105 s to 120 s) and sections with small curvature under the ''standard'' weather. Seeing that the difference between the two paths was relatively clearer in the change curvature sections, as shown in the inserted figures. It is seen that the MPC and RMPC approach was seriously affected by additive disturbances from the hard conditions and the challenged reference trajectories. Specifically, the third consideration of the segmented road is a circular road with high speed at a roundabout, which is an incredibly hazardous situation for vehicle control. Nevertheless, the performance of the proposed strategy provides the best robust performance with acceptably small tracking errors in any situation.

To further indicate the efficacy of the proposed strategy, Fig. 5 expresses the performance of the controller in terms of the cross-tracking error (CTE), which is here defined as the distance between the reference path and the actual coordinate position, i.e., $y_e = v_x \sin\theta_e + v_y \cos\theta_e$. The subfigures are inserted to show the standard deviation values for specifically each case. In the large curvature of the road, the peak CTE value of the MPC and the RMPC technique reached about 0.55 m and 0.85 m in sunny weather, respectively, as clearly shown in zoom-in figure. Furthermore, the maximum CTE value of the RMPC technique about 1.2 m and 2.4 m occurred at 90 s and 138 s in the Storm situation. And the error resulting from MPC is nearly twice RMPC in each case. Its control performance was significantly degraded when it worked with increasing both the vehicle speed and road curvature under the harder weather situation. Meanwhile, the CTE values of the proposed approach on the entire test route are mostly below 0.5 m, which can be considered acceptable on the line track with a width of 3 m. It is exhibited that the proposed control scheme provides better robustness performance over three times in the same operating condition.

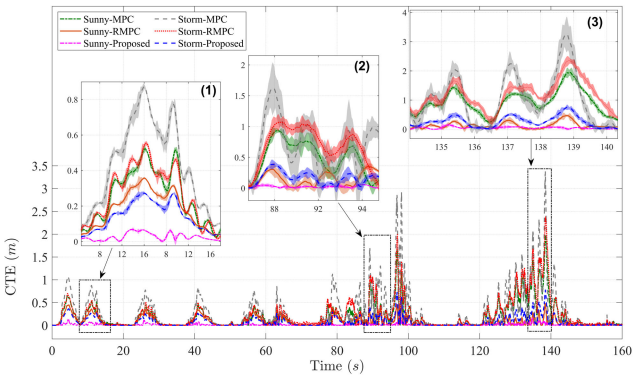

FIGURE 5. The cross tracking errors with respect to the different weather scenarios.

Fig. 6 describes the reference and responses of the longitudinal velocity profiles with respect to various scenarios, respectively. It is inserted the zoom-in figures for the three typical segment roads mentioned above explanation. Likewise, Fig. 7 is displayed its errors as the standard deviation

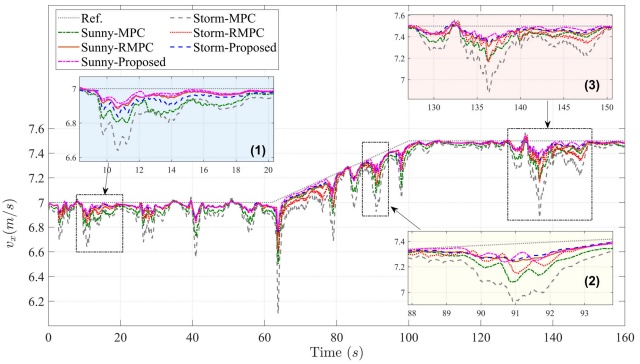

FIGURE 6. The longitudinal velocities response with respect to the various scenario.

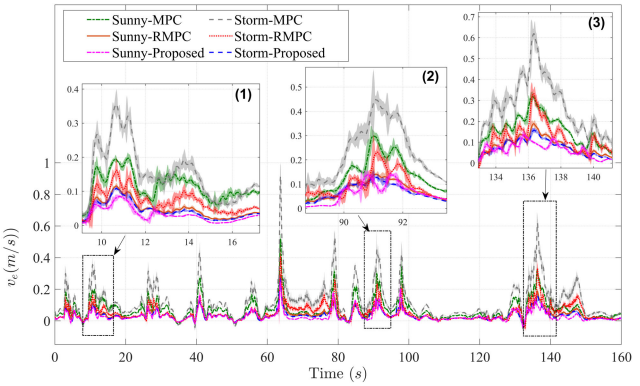

FIGURE 7. The longitudinal velocity errors response with respect to the various scenario.

indices. To these results, the response speed of the designed controller is better than those of the MPC and RMPC. In details, the MPC performance was increased with the error peak in the Sunny case nearly two times that of the Storm case, from 0.2 m/s to 0.39 m/s at 10 s, from 0.29 m/s to 0.52 m/s at 91.5 s and from 0.32 m/s to 0.69 s at 165.5 s corresponding to it happens on 1) curving road, 2) perpendicular road and 3) circular road. Meanwhile, the RMPC delivers its better robustness performance with an error peak increased from 0.1 m/s, 0.12 m/s and 0.19 m/s to 0.2 m/s, 0.23 m/s and 0.39 m/s at two weather situations, respectively. In contrast, the designed controller still maintained its merit with the peak error kept in a small range, 0.1 m/s at 10.5 s and 0.17 m/s at 136.5 s. On the whole, it is quite clear that the reference tracking performance is apparently good although a bit of error exists when changing velocity at 62 s as well as at circular curvature around 135 s, which still stays in an acceptable range. Such problems often come from neglecting the role of the traction motor variables, resulting in the control signal not being fully effective to follow the speed reference perfectly.

Fig. 8 and Fig. 9 show the time evolution of the control inputs of the front steering angle and the longitudinal acceleration, respectively. As shown in these figures, it is obvious

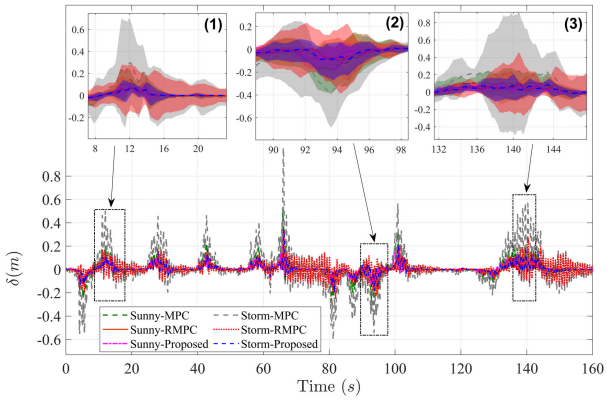

FIGURE 8. The optimal control signals of the front steering angle.

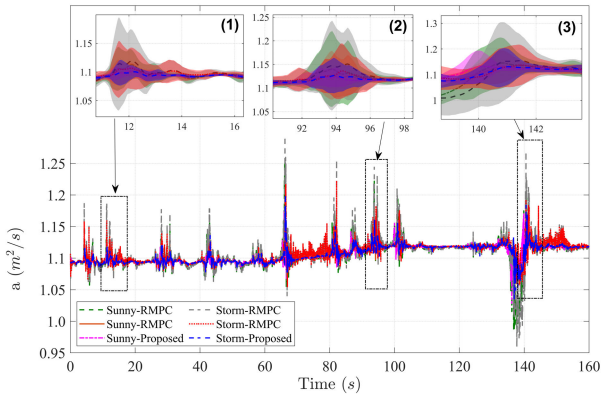

FIGURE 9. The optimal control signals of the longitudinal acceleration.

that the proposed control approach significantly reduces the control efforts. Even though the control effort signals generated by the proposed control approach are the smallest, the control performance is best in the comparative controllers. It can be observed that the input constraints are satisfied by using the proposed method. Generally, the CTE values and longitudinal velocity errors controlled by the proposed approach are concurrently near zero along the straight path (from 100 s to 120 s), but the control performances are affected by the difficulty of the scenario as the fast-changing reference (during the speed increasing period or large bend at about 138 s).

In order to have a quantitative comparison of the effectiveness by the control approaches in different scenarios, the performance indices of the cross-tracking error y_e and the longitudinal velocity error v_e in Fig. 10 are calculated by using the absolute integral error (AIE) indices [45]. The period of evaluation for each trial scenario is selected from 8 s to 10 s for 1) large curvature road (Fig. 10 (a), (b)), from 88 s to 94 s for 2) perpendicular road (Fig. 10 (c), (d)) and from 128 s to 151 s for 3) circular road in the roundabout (Fig. 10 (e), (f)). As shown in these figures, the proposed control method re-confirmed the effectiveness with the smallest AIE of the CTEs and the longitudinal velocity errors thanks to the flexible combination of the ROFC method and the AMPC approach. It enables the design of an effective controller,

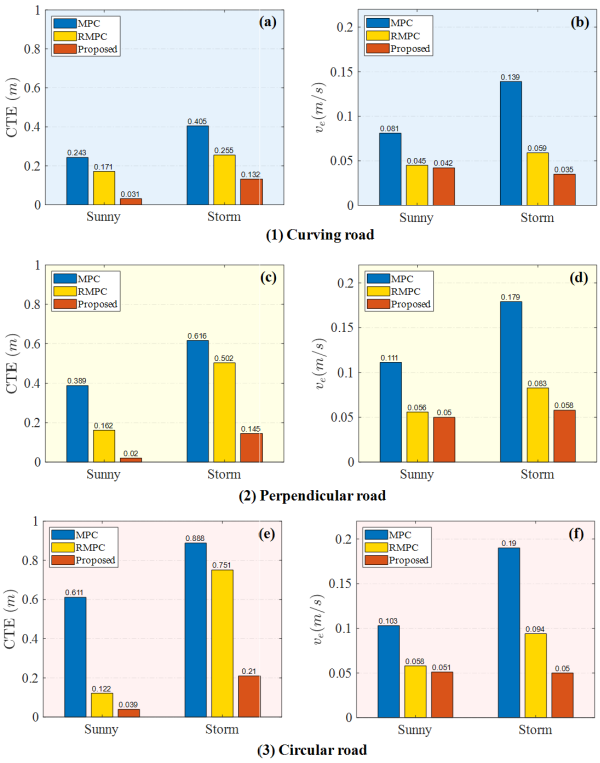

FIGURE 10. The absolute integral error indices of each trial scenario; (a), (b) large curvature road; (c), (d) perpendicular road; (e), (f) circular road in the roundabout.

which significantly outperforms the other approach with great performance and robust stabilization.

VI. CONCLUSION

This paper presented the robust adaptive path tracking control scheme for safe autonomous driving subject to parametric uncertainties and additive disturbances. To improve the accuracy, the online estimation of unknown model parameters is conducted, where the bounded estimation error is guaranteed to be nonincreasing. The integration of the interval predictors into both the ROFC approach and the AMPC-based safety controller carries out the great control performance in comparison to the RMPC approach with identical specifications. In addition, we theoretically show the stability and recursive feasibility in finite time of the controlled system by a novel nonconservative Lyapunov function. The robust stability conditions are expressed in terms of LMIs. Finally, simulation studies are conducted to verify the efficacy of the proposed method. The strategies are verified in the environmental simulation under various scenarios that display effectiveness as well as potential in practical AV applications in the future.

In the future, the proposed algorithm will be expanded in more complex operation scenarios in the presence of traffic lights, multi-lanes and multi-obstacles. More importantly, the personalization of the proposed algorithm will be focused to increase its adaptability. For instance, the target velocity will be adjusted to the different driving styles. The bounded uncertainty set will be flexibly updated. Additionally, the

RL or deep learning will be combined with the proposed algorithm.

APPENDIX A
MATHEMATICAL MODEL

Proof: Based on the non-linear embedding approach [36], [46], the linear parameter-varying matrices in (2) are obtained as

$$A = \begin{bmatrix} 0 & A_{12} & A_{13} & 0 & 0 & 0 \\ 0 & A_{22} & A_{23} & 0 & 0 & 0 \\ 0 & A_{32} & A_{33} & 0 & 0 & 0 \\ A_{41} & 0 & 1 & 0 & 0 & 0 \end{bmatrix},$$
$$B = \begin{bmatrix} B_{11} & 1 \\ B_{21} & 0 \\ B_{31} & 0 \\ 0 & 0 \end{bmatrix} \tag{22}$$

with

$$\begin{aligned} A_{12} &= \frac{C_f \sin\delta}{mv_x}, \quad A_{13} = \frac{C_f l_f \sin\delta}{mv_x} + v_y, \\ A_{22} &= -\frac{C_r + C_f \cos\delta}{mv_x}, \quad A_{23} = \frac{C_r l_r - C_f l_f \cos\delta}{mv_x} - v_x, \\ A_{23} &= \frac{C_r l_r - C_f l_f cos\delta}{Iv_x}, \quad A_{33} = \frac{C_r l_r^2 - C_f l_f^2 \cos\delta}{Iv_x}, \\ A_{41} &= \frac{v_x \cos\theta_e - v_y \sin\theta_e}{(1 - y_e\kappa)v_x}\kappa, \\ B_{11} &= -\frac{1}{m}\sin\delta C_f, \\ B_{21} &= \frac{1}{m}\cos\delta C_f, \; B_{31} = -\frac{1}{I_z}\cos\delta C_f l_f. \end{aligned} \tag{23}$$

The parameter values are given as follows: $l_f = 0.52\ m$, $l_r = 0.63\ m$, $m = 198\ kg$ and $I_z = 275.8\ kg.m^2$. ■

APPENDIX B
PROOF OF LEMMA 1

Proof: The Lyapunov function is considered in the form:

$$V_1(t) = \widetilde{\xi}^\top(t)\frac{1}{\breve{\sigma}}\widetilde{\xi}(t) \tag{24}$$

According to [47], the time derivative of V_1 is calculated as

$$\begin{aligned} \dot{V}_1(t) &= V_1(t) + \dot{\kappa}_e\left(\vartheta^2(t) - \frac{\widetilde{\delta}^2(t)}{1 + \dot{\kappa}_e\Lambda^2(t)\breve{\sigma}(t)}\right) \\ &\le V_1(t) + \dot{\kappa}_e\left(\overline{\vartheta}^2(t) - \frac{\widetilde{\delta}^2(t)}{1 + \dot{\kappa}_e\Lambda^2(t)\breve{\sigma}(t)}\right) \end{aligned} \tag{25}$$

Substituting (7) into (24), [27] one obtains:

$$\dot{V}_1(t) = V_1(t) + \dot{\varpi}^2(t) - \varpi^2(t) \tag{26}$$

In practice, we obtain $V_1(t) \le \varpi^2(t)$, meaning $\dot{V}_1(t) \le \dot{\varpi}^2(t)$ [25]. Owing to $\xi^* \in \mathcal{D}(0)$, we can give the conclusion that $\xi^* \in \mathcal{D}(t), \forall t \le 0$. Furthermore, the expressions (5c) and (7) yield $\dot{\varpi}(t)^2 - \varpi^2(t) \le 0$. As the result, (26) can be led to $\dot{V}_1(t) \le V_1(t)$. Thus, it is straightforward to confirm that $|\widetilde{\xi}|^2 \le |\widetilde{\xi}|^2$ and the boundedness of the estimation error is verified. The proof is completed. ■

APPENDIX C
PROOF OF THEOREM 1

Proof: Let the interval estimation error be defined as $\underline{e} = x - \underline{x}$ and $\overline{e} = \overline{x} - x$ then substituting them into (12), we have:

$$\begin{cases} \dot{\underline{e}}(t) = A_0\underline{e}(t) + \underline{\varsigma}_1(t) + \underline{\varsigma}_2(t), \\ \dot{\overline{e}}(t) = A_0\overline{e}(t) + \overline{\varsigma}_1(t) + \overline{\varsigma}_2(t), \end{cases} \tag{27}$$

where $\underline{\varsigma}_1 = \sum_{i=1}^{2^N}\chi_i\Xi_i x + \Xi^+\overline{x}^- + \Xi^-\overline{x}^+, \varsigma_1 = -\sum_{i=1}^{2^N}\chi_i\Xi_i x + \Xi_+\overline{x}^+ + \Xi_-\underline{x}^-, \varsigma_2 = d - \underline{d} + \overline{d}, \varsigma_2 = -d + \overline{d} - \underline{d}$.

In addition, from bounded conditions (8) and (9), we get:

$$\begin{aligned} \underline{A}^+\underline{x}^+ - \overline{A}^+\underline{x}^- - \underline{A}^-\overline{x}^+ + \overline{A}^-\overline{x}^- &\le Ax \\ &\le \overline{A}^+\overline{x}^+ - \underline{A}^+\overline{x}^- - \overline{A}^-\underline{x}^+ + \underline{A}^-\underline{x}^- \end{aligned} \tag{28}$$

Substituting (10) into (28), [27] one obtains:

$$-\Xi^+\underline{x}^- - \Xi^-\overline{x}^+ \le \sum_{i=1}^{2^N}\chi_i\Xi_i x \le \Xi^+\overline{x}^+ + \Xi^-\underline{x}^- \tag{29}$$

From the above-mentioned calculated scope, the terms $(\underline{\varsigma}_1, \overline{\varsigma}_1)$ are non-negative provided that (8) holds. Meanwhile, non-negativity or the terms $(\underline{\varsigma}_2, \overline{\varsigma}_2)$ also follow to Assumption 2. Based on [48], we have $\underline{e}(t), \overline{e}(t) \ge 0, \forall t \ge 0$, then the inclusion property (8) is confirmed. The optimization problems are performed by solving the LMI conditions, and some other expressions in (16a) are expressed as

$$\Omega = \begin{bmatrix} \Omega_{11} & \Omega_{12} & \Omega_{13} & P \\ \Omega_{12}^\top & \Omega_{22} & \Omega_{23} & Z^+ \\ \Omega_{13}^\top & \Omega_{23}^\top & \Omega_{33} & -Z^-. \\ P & Z^+ & -Z^- & -\Gamma \end{bmatrix}$$

with

$$\begin{aligned} \Omega_{11} &= \upsilon_1^\top P + P\upsilon_1 + G, \; \Omega_{22} = \upsilon_1\top H^+ + \upsilon_2 H^+ + G^+, \\ \Omega_{12} &= \upsilon_1^\top H^+ + \upsilon_2 P + F^+, \; \Omega_{23} = H^+\upsilon_3 - \upsilon_2\top H^- + G, \\ \Omega_{13} &= P\upsilon_2 - \upsilon_1^\top H^- - F^-, \; \Omega_{33} = -H^-\upsilon_3 - \upsilon_3^\top H^- + G^-, \end{aligned}$$

and

$$\Psi = \begin{bmatrix} \Psi_{11} & \Psi_{12} & \Psi_{13} & I \\ \Psi_{12}^\top & \Psi_{22} & \Psi_{23} & I \\ \Psi_{13}^\top & \Psi_{23}^\top & \Psi_{33} & -I \\ I & I & -I & -L \end{bmatrix}$$

with

$$\begin{aligned} \Psi_{11} &= P^{-1}\upsilon_1^\top + \upsilon_1 P^{-1} + \beta^\top K_1^\top + \beta K_1 + G_c, \\ \Psi_{12} &= P^{-1}\upsilon_1^\top + \upsilon_2(H^+)^{-1} + \beta K_2 + \beta^\top K_1^\top + F_c^+, \\ \Psi_{13} &= P^{-1} - \upsilon_1^\top + \upsilon_3(H^-)^{-1} + \beta U_3 + \beta^\top K_1^\top + F_c^-, \\ \Psi_{22} &= (H^+)^{-1}\upsilon_2^\top + \upsilon_2(H^+)^{-1} + \beta^\top K_1^\top + \beta K_2 + G_c^+, \\ \Psi_{23} &= -(H^+)^{-1}\upsilon_2^\top + \upsilon_3(H^-)^{-1} - \beta^\top K_2^\top + \beta K_3 + F_c, \\ \Psi_{33} &= -(H^-)^{-1}\upsilon_3^\top - \upsilon_3(H^-)^{-1} - \beta^\top K_3^\top - \beta K_3 + G_c^-. \end{aligned}$$

The conditions $P > 0$, $H^+ > 0$, $H^- > 0$ mean that the inequality (16a) is satisfied. Whilst all matrices in inequalities (16b) and (16c) have a diagonal structure, so they are equivalent under situation $G_c = P^{-1}GP^{-1}$, $G_c^+ = (H^+)^{-1}Q^+(H^+)^{-1}$, $G_c^- = (H^-)^{-1}Q^+(H^-)^{-1}$, $F_c^+ = P^{-1}F^+(H^+)^{-1}$, $F_c^- = P^{-1}F^-(H^-)^{-1}$. In addition, denoting $\Omega = M^\top \Psi M$ with $M = \begin{bmatrix} P & H^+ & H^- \end{bmatrix} I_{2p+3}$, $K_1 = \kappa_1/P$, $K_2 = \kappa_2/H^+$, $K_3 = \kappa_3/H^-$, and the condition $\Psi \preceq 0$ leads to $M \preceq 0$. As the consequence, all above conditions are confirmed for $\kappa_1 = U_1 P$, $\kappa_2 = U_2 Z^+$ and $\kappa_3 = U_3 Z^-$.

To analyze its stability in the system, the Lyapunov candidate function is considered as follows:

$$\begin{aligned} V_2 &= X^\top PX + X^\top H^+ X^+ - X^\top H^- X^- \\ &= \sum_{i=1}^{2p} P_{i,i} X_i^2 + H_{i,i}^+ |X| X_i^+ + H_{i,i}^- |X| X_i^- \end{aligned} \tag{30}$$

It is obvious that $V_2 > 0$ provided that (16a). Denoting $\widetilde{X} = [X, X^+, X^-, \widetilde{\psi}]^\top$ and taking the time derivative of the above Lyapunov function, one obtains:

$$\begin{aligned} \dot{V}_2 &= 2\dot{X}^\top PX + 2\dot{X}^\top H^+ X^+ - 2\dot{X}^\top H^- X^- \\ &= \widetilde{X}^\top \Omega \widetilde{X} - X^\top GX - (X^+)^\top G^+ X^+ \\ &\quad -(X^-)^\top G^- X^- - 2(X^+)^\top FX^- \\ &\quad -2(X^+)^\top F^+ X^- - 2(-X^-)^\top F^- X + \widetilde{\psi}^\top L \widetilde{\psi} \end{aligned} \tag{31}$$

We have $(X^+)^\top FX^- = 0$, $(X^+)^\top F^+ X \geq 0$, $(-X^-)^\top F^- X \geq 0$ for any diagonal matrix F, $F^+ \geq 0$ and $F^- \geq 0$. Besides, if $\Omega \preceq 0$, the Theorem 1 holds, then (31) is bounded as follows:

$$\begin{aligned} \dot{V}_2 &\leq -X^\top GX - (X^+)^\top G^+ X^+ - (X^-)^\top G^- X^- \\ &\quad -2(X^+)^\top F^+ X - 2(-X^-)^\top F^- X + \widetilde{\psi}^\top L \widetilde{\psi} \\ &\leq -X^\top \Theta X + \widetilde{\psi}^\top L \widetilde{\psi} \\ &= -\Upsilon V_2 + \widetilde{\psi}^\top L \widetilde{\psi} \end{aligned} \tag{32}$$

where the term Θ equals to the inequality (16b) and $\Upsilon = \min_{i \in \overline{2p}} \lambda_i(\frac{\Theta}{P + H^+ + H^-})$ with a scalar value $\lambda(\bullet)$ is an eigenvalue of $(\bullet)$.

In conclusion, it is explicit that the evidence features of V_2 and its derivative $\dot{V}_2$ confirmed that (15) is ISS [41], [49], [50] with respect to the extended input ψ. The proof is completed. ■

APPENDIX D
PROOF OF THEOREM 2

Proof: It is worth to note that the optimal control action is obtained from (14) when the initial conditions $(\underline{x}^\top(t_i), \overline{x}^\top(t_i))^\top \in \mathcal{R} \subset \mathcal{S}^2$, for some $t_i > 0$. Based on Theorem 1, the system is ISS in regarding to $X(t) = [\underline{x}^\top(t), \overline{x}^\top(t)]^\top, \forall t \geq t_i$. According to the inclusion property (8), $|X(t)| \geq |x(t)|$ for $t \geq t_i$ and $|X(t_i)| \leq |x(t_i)| + \overline{\varepsilon}$ in which $\overline{\varepsilon}$ is a positive value, the practical ISS for the successive variable of $x(t)$.

Applying the final proposed control rule for $t \in [0, T_m)$, the extended state $X(t) \in \mathcal{S}$ and $u(t) \in \mathcal{A}$ exists on this time interval. At $t = t_1 = T_m$, if $(\underline{x}^\top(t_1), \overline{x}^\top(t_1))^\top \in \mathcal{S}^2 \setminus \mathcal{R}$ (where $\underline{x}(t_1), \overline{x}(t_1)$ are calculated as in (19)), then there exists a solution to (18). Due to the designed feature of $\hat{\mathcal{D}}(t)$ and the perturbed signals $\overline{d}(t), \overline{d}(t) - \underline{d}(t)$ are non-increasing. In other words, we have the solution at t_s that is a sub-optimal branch computed at t_{s-1}, $\forall s \geq 1$. Therefore, recursive feasibility is satisfied. It is noted that $\mathcal{R}$ is a vicinity set, and the cost function (18) with ω_i is minimized inside. Additionally, when the optimal control ΔU is executed, i.e., $X(t_s + T_p) \in \mathcal{R}$ in (20) and $[\underline{x}(t_s), \overline{x}(t_s)] \subset [\underline{x}(t_{s-1} + T_m), \overline{x}(t_{s-1} + T_m)]$, then reaching $\mathcal{R}$ is in finite time $t_i \geq T_p$, i.e., $(\underline{x}^\top(t_i), \overline{x}^\top(t_i))^\top \in \mathcal{R}$. The proof is completed. ■

REFERENCES

[1] L. Hewing, K. P. Wabersich, M. Menner, and M. N. Zeilinger, "Learning-based model predictive control: Toward safe learning in control," *Annu. Rev. Control, Robot., Auto. Syst.*, vol. 3, no. 1, pp. 269–296, May 2020.

[2] V. A. Laurense, J. Y. Goh, and J. C. Gerdes, "Path-tracking for autonomous vehicles at the limit of friction," in *Proc. Amer. Control Conf. (ACC)*, Seattle, WA, USA, May 2017, pp. 5586–5591.

[3] S. Liu, Z. Hou, T. Tian, Z. Deng, and Z. Li, "A novel dual successive projection-based model-free adaptive control method and application to an autonomous car," *IEEE Trans. Neural Netw. Learn. Syst.*, vol. 30, no. 11, pp. 3444–3457, Nov. 2019.

[4] X. Li, Z. Sun, D. Cao, D. Liu, and H. He, "Development of a new integrated local trajectory planning and tracking control framework for autonomous ground vehicles," *Mech. Syst. Signal Process.*, vol. 87, pp. 118–137, Mar. 2017.

[5] L. Wang and C. L. P. Chen, "Reduced-order observer-based dynamic event-triggered adaptive NN control for stochastic nonlinear systems subject to unknown input saturation," *IEEE Trans. Neural Netw. Learn. Syst.*, vol. 32, no. 4, pp. 1678–1690, Apr. 2021.

[6] Y. Lu, C. Wen, T. Shen, and W. Zhang, "Bearing-based adaptive neural formation scaling control for autonomous surface vehicles with uncertainties and input saturation," *IEEE Trans. Neural Netw. Learn. Syst.*, vol. 32, no. 10, pp. 4653–4664, Oct. 2021.

[7] L. Brunke, M. Greeff, A. W. Hall, Z. Yuan, S. Zhou, J. Panerati, and A. P. Schoellig, "Safe learning in robotics: From learning-based control to safe reinforcement learning," *Annu. Rev. Control, Robot., Auto. Syst.*, vol. 5, no. 1, pp. 411–444, May 2022.

[8] Z. Zhu and H. Zhao, "A survey of deep RL and IL for autonomous driving policy learning," *IEEE Trans. Intell. Transp. Syst.*, vol. 23, no. 9, pp. 14043–14065, Sep. 2022.

[9] Y. Shi, C. Shen, H. Fang, and H. Li, "Advanced control in marine mechatronic systems: A survey," *IEEE/ASME Trans. Mechatronics*, vol. 22, no. 3, pp. 1121–1131, Jun. 2017.

[10] E. F. Camacho and C. Bordons, "Model predictive control," in *Advanced Textbooks in Control and Signal Processing*. London, U.K.: Springer-Verlag, 2007.

[11] D. Gu and H. Hu, "Receding horizon tracking control of wheeled mobile robots," *IEEE Trans. Control Syst. Technol.*, vol. 14, no. 4, pp. 743–749, Jul. 2006.

[12] Z. Li, W. Yuan, Y. Chen, F. Ke, X. Chu, and C. P. Chen, "Neural-dynamic optimization-based model predictive control for tracking and formation of nonholonomic multirobot systems," *IEEE Trans. Neural Netw. Learn. Syst.*, vol. 29, no. 12, pp. 6113–6122, Dec. 2018.

[13] M. Bahadorian, B. Savkovic, R. Eaton, and T. Hesketh, "Robust model predictive control for automated trajectory tracking of an unmanned ground vehicle," in *Proc. Amer. Control Conf. (ACC)*, Jun. 2012, pp. 4251–4256.

[14] J. Fleming, B. Kouvaritakis, and M. Cannon, "Robust tube MPC for linear systems with multiplicative uncertainty," *IEEE Trans. Autom. Control*, vol. 60, no. 4, pp. 1087–1092, Apr. 2015.

[15] D. Q. Mayne, S. V. Raković, R. Findeisen, and F. Allgöwer, "Robust output feedback model predictive control of constrained linear systems," *Automatica*, vol. 42, no. 7, pp. 1217–1222, Jul. 2006.

[16] H. Li and Y. Shi, *Robust Receding Horizon Control for Networked and Distributed Nonlinear Systems*, vol. 83. New York, NY, USA: Springer, 2016.

[17] H. Wang, B. Liu, X. Ping, and Q. An, "Path tracking control for autonomous vehicles based on an improved MPC," *IEEE Access*, vol. 7, pp. 161064–161073, 2019.
[18] M. Shouche, H. Genceli, V. Premkiran, and M. Nikolaou, "Simultaneous constrained model predictive control and identification of DARX processes," *Automatica*, vol. 34, no. 12, pp. 1521–1530, Dec. 1998.
[19] A. Aswani, H. Gonzalez, S. S. Sastry, and C. Tomlin, "Provably safe and robust learning-based model predictive control," *Automatica*, vol. 49, no. 5, pp. 1216–1226, 2013.
[20] H. Fukushima and R. R. Bitmead, "Robust constrained predictive control using comparison model," *Automatica*, vol. 41, no. 1, pp. 97–106, Jan. 2005.
[21] X. Bu, X. Wu, R. Zhang, Z. Ma, and J. Huang, "Tracking differentiator design for the robust backstepping control of a flexible air-breathing hypersonic vehicle," *J. Franklin Inst.*, vol. 352, no. 4, pp. 1739–1765, Apr. 2015.
[22] X. Bu, D. Wei, and G. He, "A robust constrained control approach for flexible air-breathing hypersonic vehicles," *Int. J. Robust Nonlinear Control*, vol. 30, no. 7, pp. 2752–2776, May 2020.
[23] X.-W. Bu, X.-Y. Wu, Y.-X. Chen, and R.-Y. Bai, "Design of a class of new nonlinear disturbance observers based on tracking differentiators for uncertain dynamic systems," *Int. J. Control Automat. Syst.*, vol. 13, no. 3, pp. 595–602, 2015.
[24] M. Lorenzen, M. Cannon, and F. Allgöwer, "Robust MPC with recursive model update," *Automatica*, vol. 103, pp. 461–471, May 2019.
[25] G. Tan, C. Wen, and Y. C. Soh, "Identification for systems with bounded noise," *IEEE Trans. Autom. Control*, vol. 42, no. 7, pp. 996–1001, Jul. 1997.
[26] S. Chebotarev, D. Efimov, T. Raïssi, and T. A. Zolghadri, "Interval observers for continuous-time LPV systems with L_1/L_2 performance," *Automatica*, vol. 58, pp. 82–89, Aug. 2015.
[27] D. Efimov, L. Fridman, T. Raïssi, A. Zolghadri, and R. Seydou, "Interval estimation for LPV systems applying high order sliding mode techniques," *Automatica*, vol. 48, no. 9, pp. 2365–2371, 2012.
[28] D. Efimov and T. Raïssi, "Design of interval observers for uncertain dynamical systems," *Autom. Remote Control*, vol. 77, no. 2, pp. 191–225, 2016.
[29] J.-L. Gouzé, A. Rapaport, and M. Z. Hadj-Sadok, "Interval observers for uncertain biological systems," *Ecol. Model.*, vol. 133, nos. 1–2, pp. 45–56, 2000.
[30] T. Raïssi and D. Efimov, "Some recent results on the design and implementation of interval observers for uncertain systems," *Automatisierungstechnik*, vol. 66, no. 3, pp. 213–224, 2018.
[31] V. T. H. Le, "Robust predictive control by zonotopic set-membership estimation," Ph.D. dissertation, Dept. Autom. Control, SUPELEC, Gif-sur-Yvette, France, 2012.
[32] C. Combastel, "Stable interval observers in BBC for linear systems with time-varying input bounds," *IEEE Trans. Autom. Control*, vol. 58, no. 2, pp. 481–487, Feb. 2013.
[33] Wego-Robotics. (2022). *UGV-ERP42: Unmanned Ground Vehicle-Educational Robot Platform*. [Online]. Available: https://wego-robotics.com/wego-erp42/
[34] R. Rajamani, *Vehicle Dynamics and Control* (Mechanical Engineering Series), F. F. Ling, Ed. New York, NY, USA: Springer, 2012, pp. 1–11.
[35] J. H. Jeon, R. V. Cowlagi, S. C. Peters, S. Karaman, E. Frazzoli, P. Tsiotras, and K. Iagnemma, "Optimal motion planning with the half-car dynamical model for autonomous high-speed driving," in *Proc. Amer. Control Conf.*, Washington, DC, USA, Jun. 2013, pp. 188–193.
[36] D. Rotondo, V. Puig, F. Nejjari, and M. Witczak, "Automated generation and comparison of Takagi–Sugeno and polytopic quasi-LPV models," *Fuzzy Sets Syst.*, vol. 277, pp. 44–64, Oct. 2015.
[37] A. P. Morgan and K. S. Narendra, "On the uniform asymptotic stability of certain linear nonautonomous differential equations," *SIAM J. Control Optim.*, vol. 15, no. 1, pp. 5–24, Jan. 1977.
[38] J.-J. E. Slotine and W. Li, *Applied Nonlinear Control*. Upper Saddle River, NJ, USA: Prentice-Hall, 1991.
[39] D. Efimov, T. Raïssi, S. Chebotarev, and A. Zolghadri, "Interval state observer for nonlinear time varying systems," *Automatica*, vol. 49, no. 1, pp. 200–205, 2013.
[40] D. Efimov, T. Raïssi, and A. Zolghadri, "Control of nonlinear and LPV systems: Interval observer-based framework," *IEEE Trans. Autom. Control*, vol. 58, no. 3, pp. 773–778, Mar. 2013.
[41] R. Marino, "Adaptive control of nonlinear systems: Basic results and applications," *IFAC Proc. Volumes*, vol. 28, no. 14, pp. 869–880, 1995.
[42] L. Farina and S. Rinaldi, "Theory and applications," in *Positive Linear Systems*. Hoboken, NJ, USA: Wiley, 2000.
[43] H. Michalska and D. Q. Mayne, "Robust receding horizon control of constrained nonlinear systems," *IEEE Trans. Autom. Control*, vol. 38, no. 11, pp. 1623–1633, Nov. 1993.
[44] MORAI. (2022). *Homepage of MORAI Simulator*. [Online]. Available: https://www.morai.ai/product
[45] C. P. Vo and K. K. Ahn, "An adaptive finite-time force-sensorless tracking control scheme for pneumatic muscle actuators by an optimal force estimation," *IEEE Robot. Autom. Lett.*, vol. 7, no. 2, pp. 1542–1549, Apr. 2022.
[46] J. S. Shamma, *Control of Linear Parameter Varying Systems With Applications*. Atlanta, GA, USA: Springer, 2012, pp. 3–26.
[47] R. Johnstone, C. Johnson, R. Bitmead, and B. O. Anderson, "Exponential convergence of recursive least squares with exponential forgetting factor," in *Proc. 21st IEEE Conf. Decis. Control*, Dec. 1982, pp. 994–997.
[48] H. L. Smith, *Monotone Dynamical Systems: An Introduction to the Theory of Competitive and Cooperative Systems* (Mathematical Surveys and Monographs). AZ, USA: AMS, 1995.
[49] S. N. Dashkovskiy, D. V. Efimov, and E. D. Sontag, "Input to state stability and allied system properties," *Autom. Remote Control*, vol. 72, no. 8, pp. 1579–1614, Aug. 2011.
[50] E. D. Sontag, "The ISS philosophy as a unifying framework for stability-like behavior," in *Nonlinear Control in the Year 2000*, vol. 2, A. Isidori, F. Lamnabhi-Lagarrigue, and W. Respondek, Eds. London, U.K.: Springer, 2001, pp. 443–467.

CONG PHAT VO received the B.E. degree in electrical and electronic engineering technology and the M.Sc. degree in mechatronics engineering from the Ho Chi Minh City University of Technology and Education, Vietnam, in 2013 and 2016, respectively, and the Ph.D. degree from the Department of Mechanical Engineering, University of Ulsan, Ulsan, South Korea, in 2021.

He is currently a Postdoctoral Researcher at the Department of Electrical Engineering, Ulsan National Institute of Science and Technology (UNIST), Ulsan. His research interests include optimal control, optimization, reinforcement learning, and motion planning.

JUNGEUN LEE received the B.S. degree from the School of Electrical and Computer Engineering, Ulsan National Institute of Science and Technology (UNIST), Ulsan, South Korea, in 2020, where she is currently pursuing the Ph.D. degree with the Department of Electrical Engineering.

Her research interests include intelligent transportation systems (ITS), reinforcement learning (RL), and rule-based optimal control.

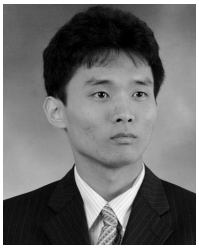

JEONG HWAN JEON received the B.S. degree in mechanical and aerospace engineering from Seoul National University, Seoul, South Korea, in 2007, and the M.S. and Ph.D. degrees in aeronautics and astronautics from the Massachusetts Institute of Technology (MIT), Cambridge, MA, USA, in 2009 and 2015, respectively.

He worked at nuTonomy (an Aptiv company since its 2017 acquisition) as a Senior Research Scientist/the Principal Research Scientist. He is currently an Assistant Professor of electrical engineering at Ulsan National Institute of Science and Technology (UNIST), Ulsan, South Korea. His current research interests include algorithmic, computational, data-based, and control-theoretic approaches to the decision making, planning and control architectures for autonomous systems, and future mobility, including self-driving cars.